

---

# The influence of microtextured basal lamina analog topography on keratinocyte function and epidermal organization

---

Brett R. Downing,<sup>1</sup> Kevin Cornwell,<sup>1,2</sup> Mehmet Toner,<sup>3</sup> George D. Pins<sup>1</sup>

<sup>1</sup>Biomedical Engineering Department, Worcester Polytechnic Institute, Worcester, Massachusetts 01609

<sup>2</sup>University of Massachusetts Medical School, Worcester, Massachusetts 01655

<sup>3</sup>Center for Engineering in Medicine and Surgical Services, Massachusetts General Hospital, Harvard Medical School, and Shriners Hospital for Children, Boston, Massachusetts 02114

Received 1 July 2004; revised 14 August 2004; accepted 16 August 2004

Published online 12 November 2004 in Wiley InterScience (www.interscience.wiley.com). DOI: 10.1002/jbm.a.30210

**Abstract:** The rational design of future bioengineered skin substitutes requires an understanding of the mechanisms by which the three-dimensional microarchitecture of tissue scaffolds modulates keratinocyte function. Microtextured basal lamina analogs were developed to investigate the relationship between the characteristic topography at the dermal–epidermal interface of native skin and keratinocyte function. Microfabrication techniques were used to create master patterns, negative replicates, and collagen membranes with ridges and channels of length scales (e.g., grooves of 50–200  $\mu\text{m}$  in depth and width) similar to the invaginations found in basal lamina at the dermal–epidermal junction of native skin. Keratinocytes were seeded on the surfaces of basal lamina analogs, and histological analyses were performed after 7 days of tissue culture at the

air–liquid interface. The keratinocytes formed a differentiated and stratified epidermis that conformed to the features of the microtextured membranes. Morphometric analyses of immunostained skin equivalents suggest that keratinocyte stratification and differentiation increases as channel depth increases and channel width decreases. This trend was most pronounced in channels with the highest depth-to-width ratios (i.e., 200  $\mu\text{m}$  deep, 50  $\mu\text{m}$  wide). It is anticipated that the findings from these studies will elucidate design parameters to enhance the performance of future bioengineered skin substitutes. © 2004 Wiley Periodicals, Inc. *J Biomed Mater Res* 72A: 47–56, 2005

**Key words:** microfabrication; skin; tissue engineering

---

## INTRODUCTION

Engineered tissue analogs composed of cultured cells, biomaterials, or composites combining them have achieved limited clinical success for the treatment of patients suffering from severe burns and chronic ulcers.<sup>1–3</sup> Yannas et al. developed a collagen–glycosaminoglycan (GAG) sponge with a silicone membrane barrier as a temporary wound covering that promotes vascularized neodermal formation.<sup>4–6</sup> Although this dermal analog has achieved some clinical success, it necessitates a second surgical procedure to reepithelialize the wound site. Boyce and his colleagues developed a composite skin substitute by laminating the surface of a collagen–GAG sponge. Fibro-

blasts were seeded into the porous collagen sponge and a flat epidermal layer was cultured on the laminated surface.<sup>7,8</sup> In clinical studies, this composite skin substitute demonstrated limited success for the treatment of full-thickness burns, although engraftment rates were suboptimal.<sup>9,10</sup> Although considerable progress has been made toward the development of analogs for repairing and restoring damaged skin, no off-the-shelf skin substitute exists that provides immediate replacement of both the lost dermis and epidermis.<sup>1</sup> The rational design of future skin substitutes must focus on the *in vitro* regulation of cellular proliferation, as well as the morphogenesis of cells into functional skin analogs that promote rapid barrier formation, reduce healing time, eliminate mechanically induced graft failure, and minimize scarring.<sup>1,11,12</sup>

Designing highly functional bioengineered skin substitutes requires an understanding of the mechanisms by which the three-dimensional architecture of tissue scaffolds modulates cellular function and regen-

Correspondence to: George D. Pins, e-mail: gpins@wpi.edu  
Contract grant sponsor: National Institutes of Health; contract grant number: P41 EB02503 (MT)  
Contract grant sponsor: Whitaker Foundation (GDP)

eration of the epidermis. Significant effort has been devoted to producing biocompatible scaffolds with defined pore sizes that help ensure proper cell–cell contacts and cell–matrix interactions, and preserve cellular function.<sup>4,5,13</sup> Although sponges and matrices with defined porosities are useful for the fabrication of relatively large and highly porous three-dimensional analogs of the extracellular matrix, future scaffolds must mimic both native tissue microstructure with cellular microenvironments (1–10  $\mu\text{m}$ ) and organ-scale structures with cellular resolution (10–1000  $\mu\text{m}$ ) to modulate cell functions that promote physiologic tissue regeneration.<sup>14,15</sup>

In native skin, an integral component of the tissue microarchitecture is the basal lamina. The basal lamina is a thin membranous layer of connective tissue found at the interdigitated interface between the dermis and the epidermis, conforming to a series of rete ridges and dermal papillae invaginations. Several studies have examined the role of basal-lamina topography on regulating keratinocyte function. In human palmar epidermis, the highest percentage (80%) of the proliferating basal and suprabasal cells is in the deeper rete ridges.<sup>16,17</sup> It has also been shown that expression of  $\alpha 2\beta 1$  integrin, a marker of epidermal stem cells, varies with topography. High expression found in patches of basal keratinocytes located on the tips of the dermal papillae (foreskin, scalp) or at the bottom of the deep rete ridges suggest that these cellular microenvironments regulate epidermal stem cell function.<sup>18–20</sup> The complex topography of the dermal–epidermal junction also enhances structural stability; in areas of the skin exposed to excessive friction (plantar and palmar surfaces), the dermal papillae and epidermal ridges are longer and more numerous.<sup>21</sup> These findings suggest that the microarchitecture of the dermal–epidermal junction influences the mechanical and structural stability of the epidermis by modulating keratinocyte proliferation and differentiation as well as cellular adhesion to the basal lamina.

To investigate the role of microtopography on keratinocyte function, a recent study described a microfabrication approach for creating basal lamina analogs with interdigitated topographies.<sup>22</sup> Channels transversed the collagen membranes with depths and widths comparable to the dimensions of native rete ridges. Skin equivalents generated with these membranes formed a differentiated and stratified epidermis with enhanced stratification in the deeper channels. The findings of this study suggest that the spatial arrangement of cell–matrix and/or cell–cell contacts is maintained by the topography of the microenvironment, providing guidance for keratinocyte differentiation and epidermal stratification.

This study further examined the relationship between membrane microtopography and keratinocyte function on the surfaces of microtextured basal lamina

analogs. A series of master patterns consisting of parallel three-dimensional channels with specific widths (50–400  $\mu\text{m}$ ) and depths (50–200  $\mu\text{m}$ ) has been designed to allow the effects of channel dimensions on keratinocyte function and epidermal reorganization to be uncoupled. The master patterns were microfabricated with the use of photolithography to enhance the fidelity between the master pattern and intended design. Use of these basal lamina analogs in skin equivalents resulted in enhanced keratinocyte stratification, proliferation, and differentiation in the channels with the greatest aspect ratios.

## MATERIALS AND METHODS

### Microfabrication of a master pattern and negative replicates

To examine the effects of membrane microtopography on keratinocyte function, master patterns consisting of parallel, three-dimensional channels (interdigitations) with widths (50–400  $\mu\text{m}$ ) and depths (50–200  $\mu\text{m}$ ), comparable to the dimensions of epidermal invaginations between dermal papillae in skin have been designed. With the use of Pro/Engineer software (PTC, Needham, MA), a high-resolution transparency mask was created by printing precise two-dimensional drawings onto acetate film (CAD/Art Service Inc, Poway, CA) with a high-resolution laser-photoplotter (Orbotech 7008MF: 20,000 dots per inch ( $\sim 1.6\text{-}\mu\text{m}$ -diameter dots). To create master patterns with varied depths, transparency masks were aligned on the surfaces of silicon wafers coated with approximately 50, 100, or 200  $\mu\text{m}$  thicknesses of SU-8 photoresist (Microchem Co., Newton, MA) and exposed to a collimated beam of UV light. The unexposed regions were dissolved in propylene glycol methyl ether acetate (PGMEA; SU-8 Developer, Microchem Co.) and the UV-crosslinked regions yielded the patterned features on the surfaces of the silicon wafers.

To create negative replicate molds, polydimethylsiloxane silicone elastomer (PDMS; Sylgard 184, Dow Corning Corp., Midland, MI) was poured onto the master pattern and polymerized by incubation at 65°C for 2 h. The polymerized PDMS overlay conformed to the fine features of the master pattern and was carefully separated from the surface. The resulting negative replicates contained surfaces of protruding ridges that were inverse replicates of the channels in the master patterns.

### Production of a basal lamina analog

To produce basal lamina analogs, small volumes of collagen–GAG coprecipitate (5 mg/mL type I collagen, 0.18 mg/mL GAG) were cast onto surfaces of micropatterned negative replicates. The white coprecipitate was prepared as previously described.<sup>23</sup> Briefly, 3.6 g of lyophilized bovine collagen (Semed S, Kensey Nash Corp., Exton PA) was

added to 600 mL 0.05M acetic-acid solution and blended at a constant temperature of 4°C for 90 min at 20,000 rpm in a refrigerated homogenizer. The coprecipitate was formed by adding 120 mL of a 0.11% w/v solution of shark cartilage chondroitin 6-sulfate (Sigma Chemical) to the blending collagen dispersion, then blending the collagen-GAG coprecipitate for an additional 90 min. The collagen-GAG dispersion was degassed by centrifugation to remove trapped air bubbles and stored at 4°C.

To create the membranes, the collagen-GAG dispersion (220–330  $\mu\text{L}/\text{cm}^2$ ) was poured onto PDMS-negative replicate, where it conformed to the surfaces. The dispersion was air dried overnight in a laminar flow hood at room temperature, and the resulting dried collagen membranes were gently peeled away from the negative replicates. Dried membranes were cross-linked by thermal dehydration at 105°C in a vacuum of less than 200 mtorr for 24 h.

### Production of a dermal analog

Composite dermal analogs consisting of a micropatterned membrane laminated on a collagen sponge were produced by methods similar to those previously described by Yannas et al.,<sup>4</sup> Boyce, Christianson, and Hansbrough,<sup>7</sup> and Pins, Toner, and Morgan.<sup>22</sup> Briefly, 10 mL of collagen-GAG dispersion was poured into an aluminum weigh pan (Fisher Scientific, Springfield, NJ), and a microfabricated membrane was floated on the surface of the dispersion. The dispersion was rapidly frozen at  $-80^\circ\text{C}$  for 1 h, placed on in a freeze dryer initially set at  $-45^\circ\text{C}$ , then lyophilized overnight (Virtis Advantage, Virtis, Inc., Gardner, NY) at a vacuum of 100 mtorr. Following lyophilization, the composites were covalently cross-linked by thermal dehydration at 105°C in a vacuum of less than 200 mtorr for 24 h, rehydrated in a 0.05M acetic acid solution for 24 h, and further crosslinked in a 0.25% glutaraldehyde solution for 24 h. The dermal analogs were then placed in 70% isopropanol for long-term storage or exhaustively washed with sterile water, PBS, and keratinocyte seeding medium (described below) for immediate use.

### Keratinocyte culture and production of skin equivalents

Normal human keratinocytes were isolated from neonatal foreskins with dispase (Gibco, Gaithersburg, MD) following the manufacturer's recommendations. The cells were propagated on a feeder layer of 3T3-J2 mouse fibroblasts (originally provided by Dr. Stelios Andreadis, State University of New York at Buffalo) as described previously.<sup>22</sup>

Keratinocytes were seeded onto the dermal analogs with methods similar to those previously described.<sup>22,24</sup> Dermal analogs were placed into 35-mm-diameter tissue culture dishes, microfabricated membrane side up, and cells in keratinocyte seeding medium (described below) were seeded onto the surface ( $5 \times 10^5$  cells/ $\text{cm}^2$ ). After 2 h, the cell-seeded dermal analogs were submerged in keratinocyte seeding medium, consisting of a 3:1 mixture of DMEM (high

glucose) (Life Technologies, Inc.–BRL) and Ham's F-12 medium (Life Technologies, Inc.–BRL) supplemented with 1% FBS (JRH Bioscience),  $10^{-10}\text{M}$  cholera toxin (Vibrio Cholerae, Type Inaba 569 B; Calbiochem, La Jolla, CA), 0.2  $\mu\text{g}/\text{mL}$  hydrocortisone (Calbiochem), 5  $\mu\text{g}/\text{mL}$  insulin (Sigma Chemical), 50  $\mu\text{g}/\text{mL}$  ascorbic acid (Sigma Chemical), and 100 IU/mL and 100  $\mu\text{g}/\text{mL}$  penicillin-streptomycin (Life Technologies, Inc.–BRL). After 24 h, the keratinocyte seeding medium was removed, and the skin equivalents were submerged for an additional 48 h in a keratinocyte priming medium composed of keratinocyte seeding medium supplemented with 24  $\mu\text{M}$  bovine serum albumin (BSA), 1.0 mM L-serine, 10  $\mu\text{M}$  L-carnitine, and a mixture of fatty acids including 25  $\mu\text{M}$  oleic acid, 15  $\mu\text{M}$  linoleic acid, 7  $\mu\text{M}$  arachidonic acid, and 25  $\mu\text{M}$  palmitic acid, all from Sigma Chemical.<sup>25</sup> After 48 h in priming medium, skin equivalents were placed on stainless-steel screens, raised to the air-liquid interface, and cultured for 7 days with an air-liquid interface medium composed of serum-free keratinocyte priming medium supplemented with 1.0 ng/mL epidermal growth factor (EGF, Collaborative Biomedical Products, Bedford, MA).

### Histological and immunohistochemistry

For histological analyses, skin equivalents were fixed in a 10% buffered formalin solution, dehydrated with increasing concentrations of ethanol, cleared with sec-butyl alcohol, and embedded in paraffin wax. Sections of skin equivalents, 6–10  $\mu\text{m}$  in thickness, were cut in a plane perpendicular to the surface of the microfabricated membranes. Sections were mounted on poly-L-lysine coated slides (Erie Scientific Company, Portsmouth, NH), stained with hematoxylin and eosin (Richard-Allan Scientific, Kalamazoo, MI), and then viewed with a Nikon Eclipse E400 microscope.

Keratinocyte proliferation and differentiation in the skin equivalents were explored by detecting the presence of Ki67, a marker for highly mitotic keratinocytes, or involucrin, a marker for terminally differentiating cells. Paraffin sections (6–10  $\mu\text{m}$ ) of skin equivalents were washed with PBS and immunostained with a staining kit (Vectastain Elite ABC; Vector Laboratories, Burlingame, CA) according to the manufacturer's recommendations. The tissue sections were deparaffinized in reverse ethanol-xylene washes, and the antigens were unmasked by digestion with 0.1% trypsin for 25 min (involucrin) or by boiling in 0.01M citrate buffer for 10 minutes (Ki67). Sections were incubated first with blocking solution (10% horse serum in PBS) for 1 h at room temperature, then with either 100  $\mu\text{L}$  of mouse monoclonal antibodies: antihuman Ki67 (1:100 dilution in blocking solution, 30 min at room temperature; Zymed Laboratories, South San Francisco, CA) or antihuman involucrin (1:8000 dilution, 1 h at 37°C; Sigma). Slides were then incubated with avidin-horseradish peroxidase (HRP) for 30 min and developed with a substrate kit (Vector Laboratories). Slides were washed five times with PBS, followed by a 5-min wash with tap water, and counterstained with hematoxylin for 55 s (Harris hematoxylin). The slides were washed with tap water for 10 min and mounted with an aqueous mounting medium (Crystal/Mount; Biomed, Foster City, CA).

## Quantitative morphometric analyses

The morphology of the microtextured skin equivalents was characterized with a Nikon Eclipse E400 microscope coupled to Spot Imaging Software. The dimensions of the collagen membranes and the thickness of the stratified epidermal layer in and between each channel were measured vertically from the lower surface of the basal layer to the outer edge of the granular layer. The thickness of the involucrin positive layer of the epidermis in each channel and between channels was measured vertically from the bottom to the top of the stained layer. The number of Ki67-positive cells were counted per unit length and used to determine the fraction of Ki67-positive cells per unit of length of basement membrane for each channel and interchannel region.

The dimensions of the master patterns were analyzed with several morphometric techniques. The depths of the 50- and 100- $\mu\text{m}$  deep features on the master patterns were measured in triplicate with a Dektak<sup>3</sup> surface profilometer (Veeco Instruments, Santa Barbara, CA), which provided two-dimensional topographic data with 0.5-nm resolution and 1-nm accuracy. The dimensions of the 200- $\mu\text{m}$ -deep features on the master pattern were measured in triplicate by focusing on the different planar surfaces of the sample with a microscope that was fitted with a calibrated dial micrometer. To determine the average shoulder-to-shoulder widths of the channels, at least 10 measurements were made on each specified channel width with the use of a Nikon SMZ-U stereo microscope coupled to Spot Imaging Software (Sterling Heights, MI).

The dimensions of the channels on PDMS negative replicates were analyzed with the Nikon Eclipse E400 microscope and Spot Imaging Software. Sections of negative replicates were cut in a plane perpendicular to the microfabricated surface with a razor blade. Sections were digitally imaged through a low-power objective lens with the microscope software. To determine the average shoulder-to-shoulder widths and maximum depths of each channel, at least five measurements were made on each of four different samples for each specified channel geometry.

## Statistical analyses

All quantitative data are reported as means plus or minus standard deviations of the mean. Correlation lines were obtained by linear regression analysis with the use of Microsoft Excel 2002.

## RESULTS

### Microtextured collagen membranes consisting of channels with defined dimensions can be created with the use of photolithography

To examine the feasibility of creating microtextured collagen membranes with topographic features that mimic native basal lamina at the dermal-epidermal

junction in skin, a series of master patterns consisting of sets of parallel channels with widths from 50 to 400  $\mu\text{m}$  and depths from 50 to 200  $\mu\text{m}$  have been designed (Fig. 1). The various channel geometries are summarized in Table I; the data for the 50- $\mu\text{m}$  W  $\times$  100  $\mu\text{m}$  D channels were omitted, as these patterns were not properly developed during the photolithography process. Samples of the master patterns, negative replicates and microtextured collagen membranes described in the Materials and Methods section are shown in Figure 1.

To determine the precision with which microfabrication techniques met the desired channel dimensions, the depths and widths of the features on the master patterns and the negative replicates were analyzed and are shown in Figure 2. It was determined that the average depths of the features on the master patterns ranged from 56.6 to 196.2  $\mu\text{m}$ . Additionally, the widths of the channels on the master patterns were determined to range from 46.5 to 379.4  $\mu\text{m}$ . These values indicated that the photolithography process faithfully replicated the original design parameters.

The accuracy with which the PDMS replicated the master pattern was determined by sectioning the PDMS and analyzing the depths, widths, and perimeters of the ridges that formed in the channels of the master pattern (Fig. 2). The ridges exhibited a trapezoidal shape, which is characteristic of channels from a master pattern that are fabricated with the use of photolithography. This shape, caused by the slight scattering of the ultraviolet light as it passed through the photoresist layer, was found to be more profound in the deeper channels. To compensate for the trapezoidal shape, the width measurement was reported as the average of the upper and lower width of each ridge (Fig. 2). When the average widths and depths of the features on the negative replicates were compared with the corresponding values on the master pattern, it was found that the PDMS reliably reproduced the topography of the master pattern (Fig. 2).

Small volumes of collagen-GAG coprecipitate cast onto the PDMS negative replicate surfaces yielded membranes that retained the patterned features of the negative replicates and were easily removed from all the PDMS molds except for those used to create channels with 200- $\mu\text{m}$  depths. On these templates, the collagen membranes were difficult to separate from the channels with the highest aspect ratio (50  $\mu\text{m}$  in width and 200  $\mu\text{m}$  in depth), and the membranes were occasionally damaged during this process. Prior to being incorporated into dermal analogs, membranes were carefully inspected and damaged or torn materials were discarded. To form dermal analogs, collagen membranes were floated on small volumes of collagen-GAG coprecipitate, frozen, lyophilized, and crosslinked. The resulting composites or dermal analogs consisted of microtextured collagen membranes laminated to collagen sponges (Fig. 1).

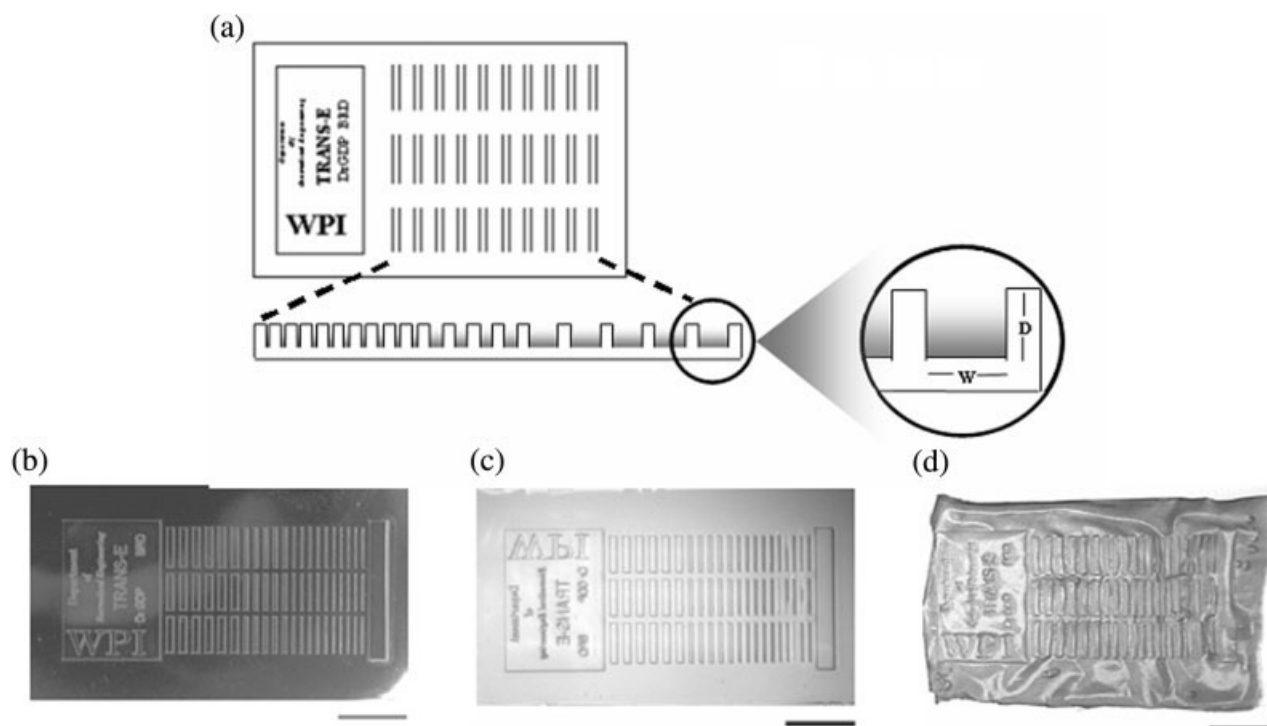


**Figure 1.** Design and microfabrication of a master pattern, a negative replicate, and a microtextured basal lamina analog. Diagram illustrating (a) the design of the master pattern, consisting of a series of parallel channels with varied widths ( $W$ ) and depths ( $D$ ). Photographs show (b) a master pattern created with the use of photolithography, (c) a negative replicate produced by polymerizing polydimethylsiloxane (PDMS) on the surface of the master pattern, and (d) a microtextured collagen membrane formed by air-drying collagen-GAG coprecipitate on the surface of the negative replicate. The scale bars represent 5.0 mm.

To characterize the fidelity with which the microtextured basal lamina analogs and dermal analogs reproduced the features on the surfaces of the PDMS negative replicates, dermal analogs were rehydrated, and quantitative morphometric analyses were conducted on the channels. Analyses of topographic features on the surfaces of the dermal analogs showed that although the microtextured collagen membranes

contained channel morphologies with distinct widths and depths (Fig. 3), the dimensions of the features vary considerably from the corresponding dimensions on the negative replicates (Table I). This variability was attributed to the relative pliability of the dermal analogs after rehydration. To more accurately compare the fidelity of the features on the membranes with the negative replicates, the perimeters of the

**TABLE I**

Specified		Master Patterns		Negative Replicates		Collagen Membranes	
Width ( $\mu\text{m}$ )	Depth ( $\mu\text{m}$ )	Width ( $\mu\text{m}$ )	Depth ( $\mu\text{m}$ )	Width ( $\mu\text{m}$ )	Depth ( $\mu\text{m}$ )	Width ( $\mu\text{m}$ )	Depth ( $\mu\text{m}$ )
50	50	42.3 $\pm$ 1.06 (10)	56.6 $\pm$ 0.16 (4)	41.0 $\pm$ 6.46 (20)	58.4 $\pm$ 2.12 (20)	71.9 $\pm$ 8.32 (20)	30.0 $\pm$ 4.17 (20)
100	50	91.1 $\pm$ 1.45 (10)	56.6 $\pm$ 0.16 (4)	92.3 $\pm$ 6.71 (20)	56.3 $\pm$ 3.56 (20)	110.0 $\pm$ 7.11 (17)	32.1 $\pm$ 3.01 (17)
200	50	176.6 $\pm$ 2.17 (10)	56.6 $\pm$ 0.16 (4)	190.7 $\pm$ 7.95 (20)	53.0 $\pm$ 6.33 (20)	188.0 $\pm$ 6.44 (11)	29.1 $\pm$ 4.45 (11)
400	50	371.0 $\pm$ 2.41 (12)	56.6 $\pm$ 0.16 (4)	390.4 $\pm$ 9.34 (24)	52.2 $\pm$ 8.82 (24)	354.8 $\pm$ 20.03 (5)	45.7 $\pm$ 5.62 (5)
100	100	79.4 $\pm$ 0.84 (10)	94.6 $\pm$ 3.89 (3)	80.5 $\pm$ 11.73 (20)	92.4 $\pm$ 6.65 (20)	113.3 $\pm$ 23.94 (19)	51.0 $\pm$ 11.85 (20)
200	100	176.5 $\pm$ 1.43 (10)	94.6 $\pm$ 3.89 (3)	182.7 $\pm$ 13.02 (20)	96.1 $\pm$ 16.18 (20)	181.8 $\pm$ 24.25 (20)	72.4 $\pm$ 8.20 (20)
400	100	370.3 $\pm$ 8.42 (12)	94.6 $\pm$ 3.89 (3)	388.1 $\pm$ 12.25 (24)	96.6 $\pm$ 8.95 (24)	358.0 $\pm$ 28.49 (23)	98.6 $\pm$ 19.77 (23)
50	200	49.4 $\pm$ 3.72 (10)	196.2 $\pm$ 8.67 (5)	46.5 $\pm$ 14.54 (20)	209.2 $\pm$ 9.05 (20)	66.8 $\pm$ 21.29 (10)	146.6 $\pm$ 10.79 (10)
100	200	94.4 $\pm$ 8.30 (10)	196.2 $\pm$ 8.67 (5)	97.4 $\pm$ 14.73 (20)	203.0 $\pm$ 5.05 (20)	117.2 $\pm$ 40.87 (19)	143.1 $\pm$ 21.78 (18)
200	200	184.9 $\pm$ 11.42 (10)	196.2 $\pm$ 8.67 (5)	193.0 $\pm$ 15.95 (20)	192.2 $\pm$ 7.60 (20)	192.3 $\pm$ 25.64 (20)	151.6 $\pm$ 14.32 (20)
400	200	396.8 $\pm$ 9.88 (12)	196.2 $\pm$ 8.67 (5)	390.6 $\pm$ 15.96 (24)	188.4 $\pm$ 7.32 (24)	368.4 $\pm$ 48.35 (24)	176.1 $\pm$ 19.52 (24)

Values are reported as means  $\pm$  standard deviations of the means; values in parentheses indicate the number of replicates measured for each parameter.

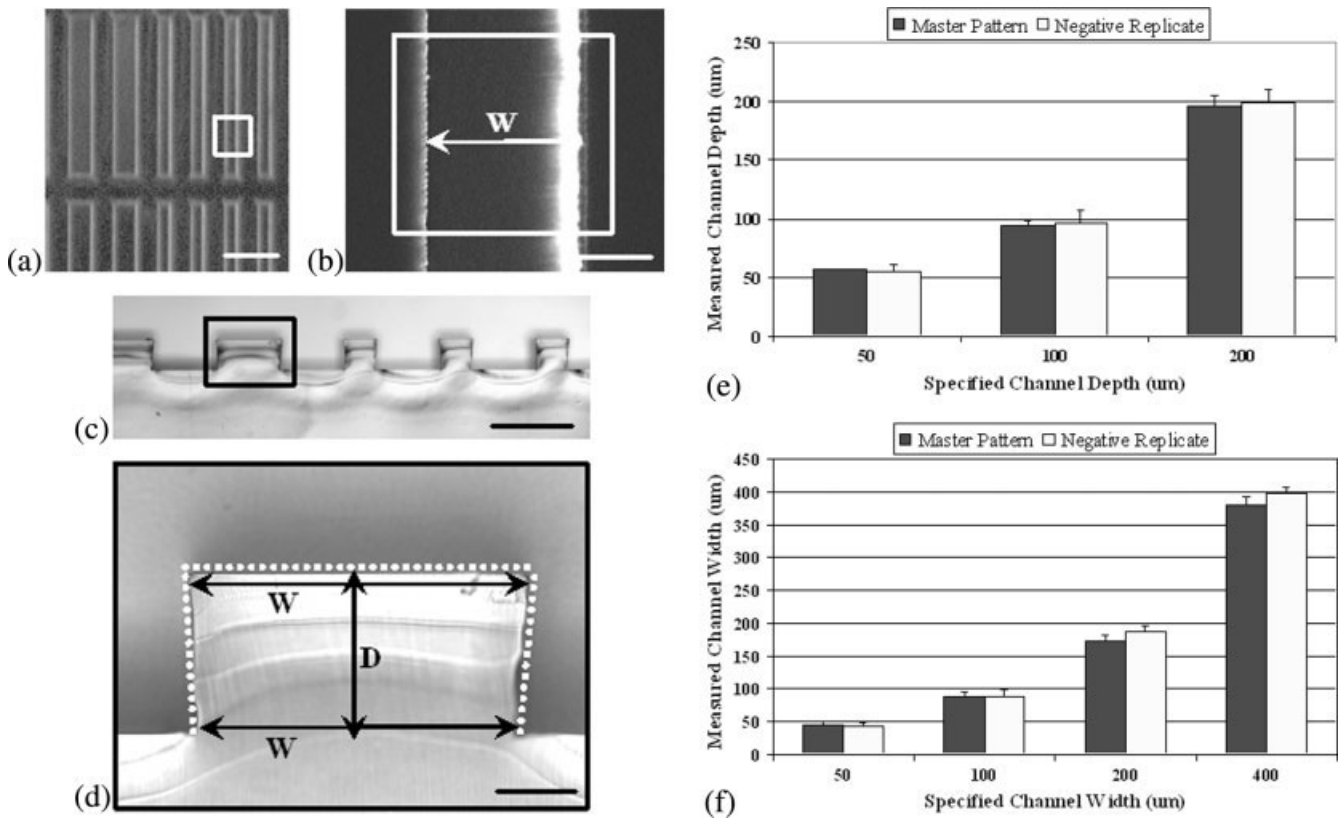


**Figure 2.** Morphometric analyses of master pattern and negative replicate. Photograph showing (a) a low-magnification view of channels on the surface of a master pattern with a box highlighting a typical region of interest for analysis. (b) High-magnification view of the region of interest on the master pattern showing the parameter used to measure channel width ( $W$ ). (c) Low-magnification image showing a section cut perpendicular to the surface of a PDMS negative replicate with a box highlighting a typical region of interest for analysis. (d) High-magnification view of a typical channel on a PDMS negative replication showing parameters used to measure channel perimeter (dotted line), channel widths ( $W$ ), and channel depth ( $D$ ). Graphs comparing the (e) average depth and (f) width measurements of the negative replicates, the master patterns, and the original design specifications. Data points represent means  $\pm$  standard deviations. Scale bars represent (a) 1.0 mm, (b) 100  $\mu\text{m}$ , (c) 500  $\mu\text{m}$ , (d) 100  $\mu\text{m}$ .

channels were measured and compared with the perimeters of the PDMS negative replicates. This analysis showed that there was a strong linear correlation ( $r^2 = 0.992$ ) between the microtextured features on the surfaces of the collagen membranes and the corresponding patterns on the surfaces of the negative replicates (Fig. 3).

### Channel dimensions influence epidermal organization

To investigate how specific channel dimensions mediate cellular organization of an epidermal layer, cultured keratinocytes were seeded on the microtextured surfaces of the dermal analogs. Histological analyses of hematoxylin and eosin-stained sections of the grafts showed that the cells formed a continuous stratified and differentiated epidermal layer that conformed to the channels as well as to the flat regions between the channels of the dermal analogs (Fig. 4).

To quantitatively analyze epidermal organization as a function of channel size, epidermal thickness was measured as the distance from the bottom of the stratum basale up through the stratum granulosum (Fig. 4). These measurements revealed several trends (Fig. 5). As channel width decreased, epidermal thickness appeared to increase. This phenomenon was most pronounced in channels that were designed to be 200  $\mu\text{m}$  deep, where the epidermal thickness increased twofold, from 82  $\mu\text{m}$  thick in 350- $\mu\text{m}$ -width channels to 182.4  $\mu\text{m}$  thick in 50- $\mu\text{m}$ -width channels. Epidermal thickness was also found to increase as channel depth increased, and all channels featured a thicker epidermis than the flat regions between channels. Comparing 50- $\mu\text{m}$ -wide channels, the epidermal thickness was 182.4  $\mu\text{m}$  in channels designed to be 200  $\mu\text{m}$  in depth and 71.3  $\mu\text{m}$  in channels designed to be 50  $\mu\text{m}$  in depth (Fig. 5). The flat interchannel regions were found to have epidermis thicknesses averaging 47  $\mu\text{m}$  (data not shown).

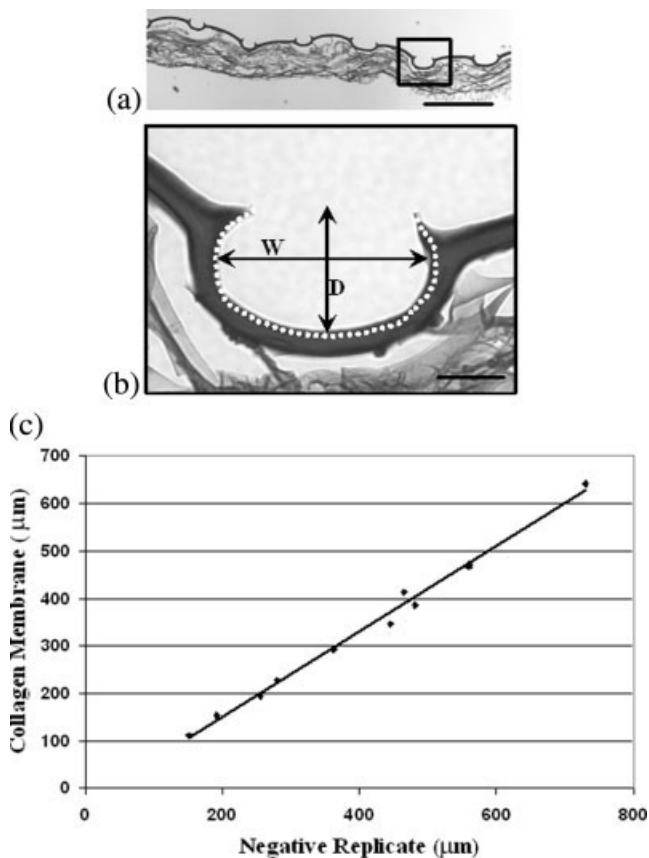


**Figure 3.** Morphometric analyses of composite dermal analogs with microtextured collagen membranes. Micrographs showing (a) a low-magnification image of a hematoxylin and eosin-stained section cut perpendicular to the surface of a dermal analog containing a microtextured dermal analog, and (b) a high-magnification image of the channel highlighted in (a). The high-magnification image shows the parameters used to measure channel width ( $W$ ), depth ( $D$ ), and perimeter (dotted line). (c) Morphometric analysis comparing the perimeter of each channel of the collagen membrane with the perimeter of the corresponding PDMS negative replicate. Perimeters of collagen membranes and negative replicates were measured in triplicate. For linear regression line,  $r^2 = 0.992$ . Scale bars represent (a) 500  $\mu\text{m}$ , and (b) 50  $\mu\text{m}$ .

### Channel dimensions influence keratinocyte function

To investigate the mechanism mediating the increase in epidermal thickness in channels with deeper and narrower dimensions, the distribution and function of cells along the microtextured surfaces of the grafts were analyzed at Day 1 in culture. The purpose of this analysis was to determine if epidermal thickness was related to an uneven cell distribution or cell packing associated with the initial cell seeding on the microtextured surfaces of the dermal analogs. Histological analysis showed that there was a uniform distribution of keratinocytes both on the surfaces of the collagen membranes and in the channels, regardless of

channel dimensions (data not shown). This suggests that the channel dimensions and not the initial cell-seeding conditions influence the proliferation and differentiation of keratinocytes.

### Cellular microenvironments influence keratinocyte differentiation

To determine how channel size affects keratinocyte proliferation and differentiation, the grafts were embedded in paraffin at Day 10 in culture and immunostained with antibodies for Ki67 and involucrin. Ki67 is a marker for highly mitotic keratinocytes, and involucrin is a marker for terminally differentiating keratinocytes. The Ki67 immunostain revealed few mitotically active cells within the epidermis in all channels and interchannel regions. However, the thickness of the involucrin positive regions of the epidermis (Fig. 4) varied with channel dimensions (Fig. 5). Similar to the relationships found with epidermal thickness and channel dimensions, the thickness of the involucrin positive region increased as channel depth increased and as channel width decreased. Additionally, all channels exhibited thicker involucrin positive regions than the flat control regions between channels. These findings suggest that the microenvironment created by the channels influences the rate of keratinocyte terminal differentiation.

## DISCUSSION

The goal of this study was to investigate the relationship between membrane microtopography and keratinocyte function on the surfaces of microtextured basal lamina analogs. A biomimetic design strategy and microfabrication techniques were used to create a series of master patterns and negative replicates consisting of parallel channels with dimensions comparable to those at the dermal–epidermal junction of native skin. Negative replicates were used as templates to produce microtextured basal lamina analogs with topographic features that closely replicated the original master patterns. These membranes were integrated into dermal analogs and seeded with keratinocytes to form skin equivalents with microtextured surfaces. Histological analyses of the skin equivalents showed that the keratinocytes form a stratified epidermal layer that conforms to the topographic features on the surfaces of the membranes. Furthermore, morphometric analyses of immunostained skin equivalents indicated that keratinocyte stratification and differentiation increases as channel depth increases and channel width decreases. This trend was most pronounced

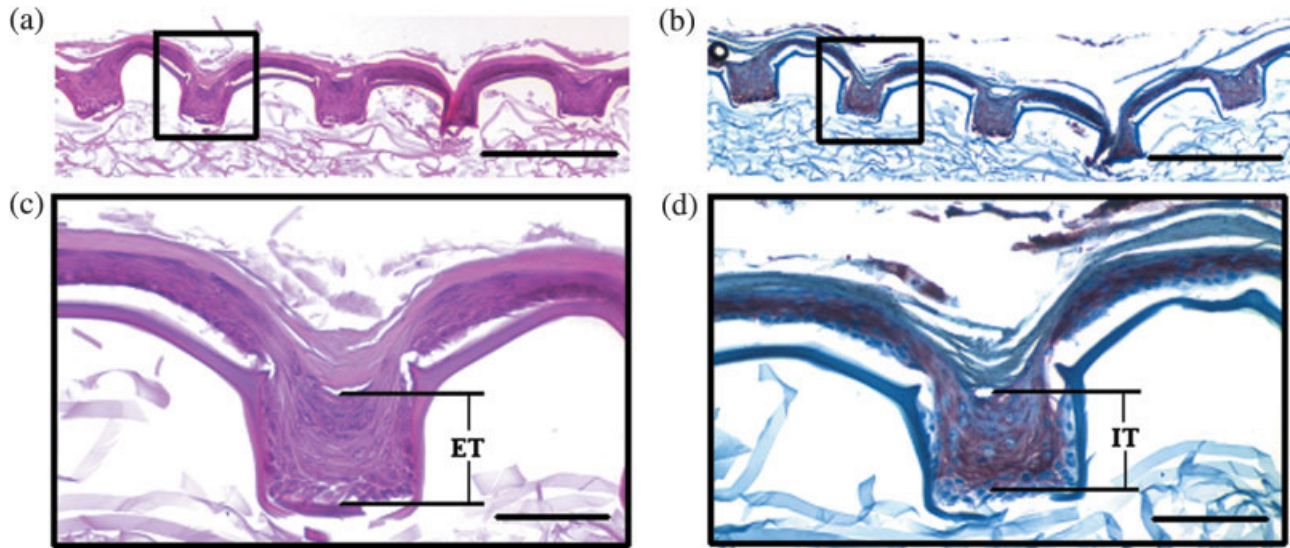


**Figure 4.** Skin equivalent with a microtextured collagen membrane. Keratinocytes were seeded on the surface of a composite dermal analog and grown at the air/liquid interface for 7 days. (a) Low-magnification micrograph of a hematoxylin and eosin-stained section of a skin equivalent with a series of micropatterned channels. (b) Low-magnification micrograph of a skin equivalent immunostained for involucrin. (c) High-magnification micrograph shows differentiated and stratified keratinocytes conforming to features on the surfaces of a channel as well as the parameter used to measure epidermal thickness (ET). (d) High-magnification micrograph shows parameter used to measure the thickness of involucrin positive epidermis (IT) within each channel. Scale bars represent 500  $\mu\text{m}$  (a), (b); 50  $\mu\text{m}$  (c), (d).

in channels with the greatest depth-to-width aspect ratios.

Photolithography and replica molding techniques were used in this study to generate the master patterns and templates needed to produce microtextured basal lamina analogs. In a previous study, master patterns were created by laser micromachining a polyimide chip. Although this technique is extremely useful for generating a wide range of widths and depths within a single pattern, a satisfactory degree of accuracy was not achieved.<sup>22</sup> The results of the morphometric analyses conducted on the master patterns and negative replicates in this study suggest that photolithography is a more reliable technique for faithfully incorporating microtextured features into collagen membranes. This allowed better investigation of the relationship between membrane microtopography and keratinocyte function on the surfaces of basal lamina analogs.

In native skin, cellular microenvironments produced by the topographic features at the dermal-epidermal junction appear to regulate the spatial organization and function of keratinocytes.<sup>16–20</sup> In thin epidermal skin, such as foreskin, breast, and scalp, clusters of keratinocyte stem cells are found at the peaks of dermal papillae. Each stem cell divides to give rise to another stem cell and a transient amplifying cell that laterally migrates down into the rete ridges. In the rete ridges transient amplifying cells undergo 3–4 divisions producing postmitotic cells that migrate up from the basal layer to form differentiated features of the tissue. In thicker epidermal skin,

however, the dermal papillae and rete ridges are longer, with clusters of epidermal stem cells found at the bottom of the rete ridges. Transient amplifying cells migrate up the basal layer as they produce postmitotic cells that, in turn, migrate to the surface of skin over a period of weeks, where they are eventually sloughed off. Although these cellular events are well characterized in native tissue, the underlying physiological or topographical mechanisms that mediate these events remain unclear.

The present study demonstrates a systematic design approach intended to establish quantitative links between the proliferation and differentiation of keratinocytes and precise variations in membrane microtopography. To probe the kinetics of keratinocyte stratification and differentiation in defined cellular microenvironments, sections of skin equivalents were immunostained with involucrin, a marker of terminal differentiation. Involucrin is normally expressed only in the upper layers of the epidermis, but during the early stages of wound healing or hyperproliferation, involucrin expression can be detected in the suprabasal layer of the epidermis of skin substitutes.<sup>24,26,27</sup> The results of this study indicate that involucrin expression is most pronounced in channels with the greatest aspect ratios. These initial findings suggest that deeper and narrower topographic features promote keratinocyte differentiation and the formation of a stratified epidermal layer.

To examine the effects of cellular microenvironments on keratinocyte proliferation, sections of skin

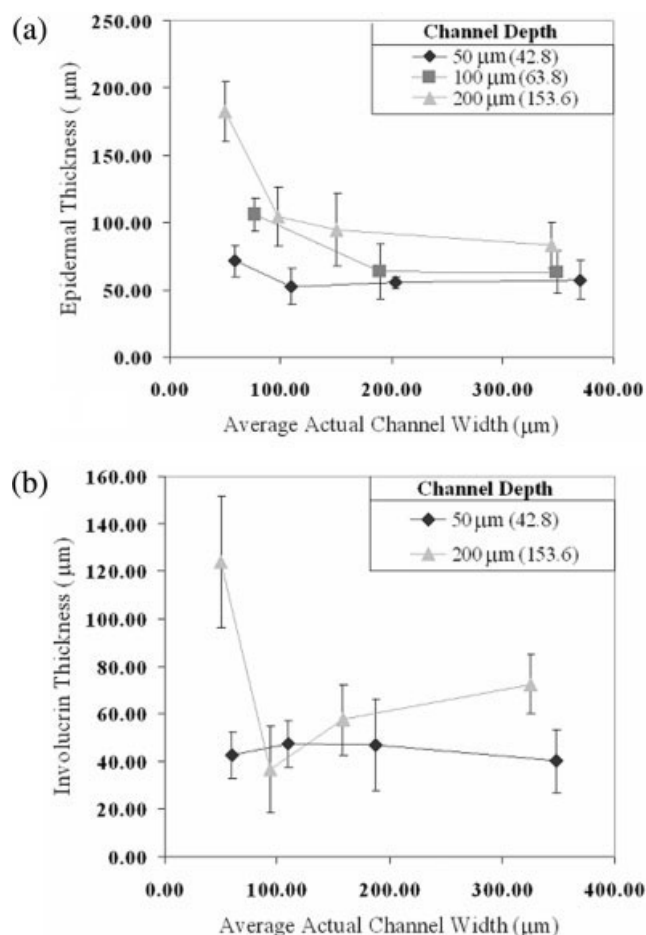


**Figure 5.** Morphometric analyses of epidermal layers cultured on microtextured collagen membranes. Graphs comparing (a) the epidermal thickness and (b) involucrin positive epidermal thicknesses with membrane channel widths for various specified channel depths. Symbols represent specified channel depths. Actual mean channel depths are shown in parentheses. Data points represent means plus or minus standard deviations.

equivalents were immunostained with Ki67, a marker for basal and suprabasal cell proliferation. This investigation identified little evidence of mitotically active cells in any of the channels or the interchannel spaces of the skin equivalents. These findings suggest that the current model system may not promote the clustering of highly proliferative stem cells within the microtopographic surface features of the dermal analogs.

A recent study showed that the presence of epidermal stem cells on the surfaces of collagen matrices may depend, in part, on paracrine signaling from dermal fibroblasts.<sup>28</sup> In the presence of fibroblasts, keratinocyte proliferation is stimulated and epidermal morphology is improved.<sup>28,29</sup> These interactions may be mediated through paracrine signaling with cytokines such as keratinocyte growth factor (KGF), a fibroblast-secreted growth factor that regulates epithelial cell growth. Ponc and his colleagues found that

when keratinocytes were cultured on scaffolds in the absence of fibroblasts, no proliferative cells were detected within the epidermis after 2 weeks at the air/liquid interface, and this epidermis consisted of only three to four viable cell layers. It is interesting to note that the findings from this study are consistent with an analysis of the epidermal layer that formed in the flat, interchannel regions of the dermal analogs after 1 week at the air/liquid interface. The absence of highly proliferative keratinocyte stem cells on the surfaces of these skin equivalents may be due to the absence of fibroblasts in this model system. A study examining the effects of fibroblasts on keratinocyte function in this model system is currently under way.

Incorporating basal lamina analogs into the future design of skin equivalents will enhance their performance and healing potential by providing functions associated with the microstructural features at the dermal–epidermal interface. The topography found at the dermal–epidermal junction in native skin is believed not only to affect the spatial organization of the epidermis, but also to aid in dermal–epidermal adherence and transport of nutrients from the dermis to the epidermis. The results from this study and future studies involving microtextured skin equivalents may be useful for identifying the membrane dimensions that promote the most rapid regeneration of mature, robust epidermis.

The authors wish to thank Octavio Hurtado in the Center for Engineering in Medicine at Massachusetts General Hospital (MGH) for his expert assistance in microfabricating the master patterns, the Department of Obstetrics and Gynecology at UMMS (Worcester, MA) for providing us with neonatal foreskins, and Dr. Russell Kronengold at Kensey Nash Corp. (Exton, PA) for his generous donations of the collagen materials that were used to produce the dermal analogs. The authors also thank Sarah Walsh and Alex Aimetti for their technical assistance in making countless morphometric measurements. Microfabrication was performed at the BioElectroMechanical Systems (BioMEMS) Resource Center, MGH.

## References

1. Sheridan RL, Tompkins RG. Skin substitutes in burns. *Burns* 1999;25:97–103.
2. Teumer J, Hardin-Young J, Parenteau NL. Tissue engineered skin. In: Patrick CW Jr, Mikos AG, McIntire LV, editors. *Frontiers in tissue engineering*. New York: Pergamon; 1998. p 664–677.
3. Phillips TJ. New skin for old: Developments in biological skin substitutes. *Arch Dermatol* 1998;134:344–349.
4. Yannas IV, Burke JF, Gordon PL, Huang C, Rubenstein RH. Design of an artificial skin. II. Control of chemical composition. *J Biomed Mater Res* 1980;14:107–131.
5. Yannas IV, Burke JF, Orgill DP, Skrabut EM. Wound tissue can utilize a polymeric template to synthesize a functional extension of skin. *Science* 1982;215:174–176.

6. Heimbach D et al. Artificial dermis for major burns. *Ann Surg* 1988;208:313–320.
7. Boyce ST, Christianson DJ, Hansbrough JF. Structure of a collagen–GAG dermal skin substitute optimized for cultured human epidermal keratinocytes. *J Biomed Mater Res* 1988;22:939–957.
8. Boyce ST, Hansbrough JF. Biologic attachment, growth and differentiation of cultured human epidermal keratinocytes on a graftable collagen and chondroitin-6-sulfate substrate. *Surgery* 1988;103:421–430.
9. Hansbrough JF, Boyce ST, Cooper ML, Foreman TJ. Burn wound closure with cultured autologous keratinocytes and fibroblasts attached to a collagen–glycosaminoglycan substrate. *J Am Med Assoc* 1989;262:2125–2130.
10. Boyce ST, Goretsky MJ, Greenhalgh DG, Kagan RJ, Rieman MT, Warden GD. Comparative assessment of cultured skin substitutes and native skin autograft for treatment of full-thickness burns. *Ann Surg* 1995;222:743–752.
11. Boyce ST. Cultured skin substitutes: a review. *Tissue Eng* 1996;2:255–266.
12. Parenteau NL, Hardin-Young J, Ross RN. Skin. In: Lanza RP, Langer R, Vacanti J, editors. *Principles of tissue engineering*. San Diego, CA: Academic; 2000. p 879–890.
13. Yannas IV, Lee E, Orgill DP, Skrabut EM, Murphy GF. Synthesis and characterization of a model extracellular matrix that induces partial regeneration of adult mammalian skin. *Proc Natl Acad Sci U S A* 1989;86:933–937.
14. Bhatia SN, Chen CS. Tissue engineering at the micro-scale. *Biomed Microdev* 1999;2:131–144.
15. Desai T. Micro- and nanoscale structures for tissue engineering constructs. *Med Eng Phys* 2000;22:595–606.
16. Lavker RM, Sun TT. Heterogeneity in epidermal basal keratinocytes: Morphological and functional correlations. *Science* 1982;215:1239–1241.
17. Lavker RM, Sun TT. Epidermal stem cells. *J Invest Dermatol* 1983;81:121s–127s.
18. Carter WG, Symington BE, Kaur P. Cell adhesion and the basement membrane in early epidermal morphogenesis. In: Fleming TP, editor. *Epithelial organization and development*. London: Chapman and Hall; 1992. p 299–327.
19. Jones PH, Harper S, Watt FM. Stem cell patterning and fate in human epidermis. *Cell* 1995;80:83–93.
20. Jensen UB, Lowell S, Watt FM. The spatial relationship between stem cells and their progeny in the basal layer of human epidermis: A new view based on whole-mount labelling and lineage analysis. *Development* 1999;126:2409–2418.
21. Odland GF. The morphology of the attachment between the dermis and the epidermis. *Anat Record* 1950;108:399–413.
22. Pins GD, Toner M, Morgan JR. Microfabrication of an analog of the basal lamina: biocompatible membranes with complex topographies. *FASEB J* 2000;14:593–602.
23. Chamberlain LJ, Yannas IV. Preparation of collagen–glycosaminoglycan copolymers for tissue regeneration. In: Morgan JR, Yarmush ML, editors. *Tissue engineering methods and protocols*. Totowa, NJ: Humana Press; 1998. p 3–17.
24. Medalie DA, Eming SA, Collins ME, Tompkins RG, Yarmush ML, Morgan JR. Differences in dermal analogs influence subsequent pigmentation, epidermal differentiation, basement membrane, and rete ridge formation of transplanted composite skin grafts. *Transplantation* 1997;64:454–465.
25. Boyce ST, Williams ML. Lipid supplemented medium induces lamellar bodies and precursors of barrier lipids in cultured analogues of human skin. *J Invest Dermatol* 1993;101:180–184.
26. Gibbs S, Pinto ANS, Murli S, Huber M, Hohl D, Ponc M. Epidermal growth factor and keratinocyte growth factor differentially regulate epidermal migration, growth and differentiation. *Wound Rep Reg* 2000;8:192–203.
27. Watt FM. Involucrin and other markers of keratinocyte terminal differentiation. *J Invest Dermatol* 1983;81:100s–103s.
28. el-Ghalbzouri A, Gibbs S, Lamme E, Van Blitterswijk CA, Ponc M. Effect of fibroblasts on epidermal regeneration. *Br J Dermatol* 2002;147:230–243.
29. Smola H, Thiekotter G, Fusenig NE. Mutual induction of growth factor gene expression by epidermal–dermal cell interaction. *J Cell Biol* 1993;122:417–429.